Accepted Manuscript

Design and characterisation of cellular composite structures for automotive crash-boxes manufactured by out of die ultraviolet cured pultrusion

I. Saenz-Dominguez, I. Tena, A. Esnaola, M. Sarrionandia, J. Torre, J. Aurrekoetxea

PII: S1359-8368(18)30689-9

DOI: 10.1016/j.compositesb.2018.10.046

Reference: JCOMB 6125

To appear in: *Composites Part B*

Received Date: 1 March 2018

Revised Date: 12 September 2018

Accepted Date: 14 October 2018

Please cite this article as: Saenz-Dominguez I, Tena I, Esnaola A, Sarrionandia M, Torre J, Aurrekoetxea J, Design and characterisation of cellular composite structures for automotive crash-boxes manufactured by out of die ultraviolet cured pultrusion, *Composites Part B* (2018), doi: https://doi.org/10.1016/j.compositesb.2018.10.046.

Design and characterisation of cellular composite structures for automotive crash-boxes manufactured by out of die ultraviolet cured pultrusion

I. Saenz-Dominguez [a*], I. Tena [a], A. Esnaola [a], M. Sarrionandia [a], J. Torre [b], J. Aurrekoetxea [a]

[a] *Mechanical and Industrial Production Department; Mondragon Unibertsitatea, Loramendi 4, 20500 Mondragón, Spain.*

[b] *Irurena Group, Ctra. de Tolosa s/n, 20730 Azpeitia, Spain.*

[*]Corresponding author. Tel.: +34 664 256 879; e-mail: isaenz@mondragon.edu

Abstract

The present paper analyses the feasibility of designing a honeycomb-like crash-box, as a cellular structure, based on data obtained from the characterisation of the building block. In order to generalise the conclusions of the study, different thicknesses and testing velocities have been analysed. The main conclusion is that, if the same thickness and testing velocity are used, the specific energy absorption (*SEA*) and peak load values are similar for the building block and the crash-box. Consequently, the design of the complex structure can be validated by simplifying the test procedure. However, special attention must be put on the testing velocity, since the broken fibre percentage is higher in quasi-static conditions. Thus, *SEA* in quasi-static conditions is higher than in dynamic conditions, 64 kJ/kg and 45 kJ/kg respectively.

Keywords: A. Glass fibres, B. Impact behaviour, D. Mechanical testing, E. Pultrusion.

1. Introduction

In the last decades, lightweighting has become an important concern in the automotive industry, aiming for a reduction of CO_2 emissions in internal combustion engines cars and for an increased range in electric cars. However, this weight reduction must not result in a reduction of the safety of the passengers in crash scenarios. Therefore, materials with high impact energy absorption capabilities are demanded to fulfil safety and lightweighting requirements. Hence, composite materials are being widely studied for automotive applications [1]. The high specific energy absorption (*SEA*) capability of composite materials has been demonstrated by the research studies of many authors [2–7]. While metallic structures are designed to absorb energy by plastic deformation through progressively buckling as the column walls collapse; the absorption mechanism of composites structures is based on the progressive material collapse in a brittle manner [8]. Many researchers have demonstrated that *SEA* values of composites structures are above 45 kJ/kg, depending on the geometry and the material [2,9,10]. However, a stable and progressive collapse of the composite structures has to be ensured, since the *SEA* values are dramatically reduced if the collapse is catastrophic [11].

Therefore, a progressive collapse is the first key point of a composite crash-box design. Many authors have demonstrated the importance of the geometry in the energy absorption performance of composite crash-boxes [7,12,13]. The most common geometry in real applications is the square-sectioned tubular crash structure due to assembly and integration feasibility. However, circular impact structures are the preferred cross-section from the performance point of view [14]. As the energy absorption capability of the hexagonal structures is between the circular and square tubes [14,15], the strategy proposed by Esnaola *et al.* [16] is an alternative solution when looking for a good compromise between integration and performance. This strategy consists of assembling semi-hexagonal profiles following a honeycomb concept. Indeed, the same semi-hexagonal profile can be used as a modular building block of a cellular composite structure [17] to fulfil different crashworthiness requirements.

The second key point of a composite crash-box design for the automotive industry is the cost-effectiveness of the manufacturing process. The limited productivity of some composite manufacturing processes and the related operative costs are an obstacle to expand the use of composites in high-volume automotive applications. Nonetheless, the out of die ultraviolet (UV) cured pultrusion has recently been proposed as a new cost-effective manufacturing process [18–20]. The productivity rate of this process is

increased compared to the traditional pultrusion without reducing the mechanical properties of the pultruded profiles [18].

The third key point is the prediction of the energy absorption performance of the composite crash-box. It is certainly true that the response of pultruded composite tubes under axial compression has been widely investigated by many researchers [15,21]. Indeed, analysing the behaviour of the composite subjected to axial compressive loads is the most extended way to evaluate the suitability of a composite material for crashworthy applications [22]. These axial compression tests can be carried out at quasi-static and dynamic compressive conditions, but they may show different trends of the effect of impact velocity on energy absorption capability of composites [23]. In case of designing crash-boxes using honeycomb concept, the uncertainty is even higher. The challenge is to probe if the energy absorption capability of this building block can be individually qualified; and as a cellular material, the periodic nature of their assemblies simplifies the analysis and prediction of their behaviour [17].

Hence, this paper deals with the prediction of the energy absorption performance of out of die UV cured pultruded crash-boxes based on the assembly of semi-hexagonal profiles (building blocks). The design process of a cellular composite crash-box is analysed, comparing the energy absorption capability of the semi-hexagonal building block and the final component at quasi-static and dynamic compression rates. The effect of parameters such as the composite thickness, impact velocity and component geometry have been analysed. It is expected that the information provided in this research study contributes to developing new guidelines on designing and characterising cellular composite crash-boxes.

2. Experimental procedure

2.1. Materials

The composite used in this study is a glass/UV cured vinyl ester composite. The reinforcement consists of 300 g/m^2 and 75 mm width quasi-unidirectional E-glass tape. The reinforcement is described as quasi-unidirectional because of 8% of fibres are oriented at 90º to maintain the cohesion of the unidirectional fibres. Furthermore, these fibres are woven with the longitudinal fibres. The resin is UV curable vinyl ester supplied by Irurena S.A., whose commercial name is IRUVIOL GFR-17 LED. The photoinitiator systems is a combination of Bis (2,4,6-trimethylbenzoyl)-phenylphosphine oxide (BAPO) and 2-Dimethylamino-2-(4-methyl-benzyl)-1-(4-morpholin-4-yl-phenyl)-butan-1-one (α aminoketone).

2.2. Specimen geometry

The basic geometry (building block) of the specimens used in this study was obtained from semi-hexagonal profiles of 1.5 mm (6 glass layers) and 2 mm (8 glass layers) of thickness (Fig. 1a). The linear density of the building blocks is 0.21 kg/m and 0.28 kg/m respectively, and the fibre volume fraction of both thicknesses is the same, approximately 52%. Through the combination of building blocks, a crash-box structure can be obtained (Fig. 1b), which has demonstrated to be an efficient geometry for energy absorbing structures [16]. The assembly of the crash-box structure is based on stacking basic building blocks by adhesive joining (Hysol Loctite EA 9466 ® adhesive). In order to ensure a stable and progressive crushing of the structure a 45º chamfer type trigger is machined in the upper side of each specimen [24].

Insert Fig. 1

2.3. Manufacturing process

All the specimens were manufactured by out of die UV cured pultrusion machine (Fig. 1c), which has been developed entirely by the research group at Mondragon University. The impregnation was done in an open resin bath system and the pull system is a Kuka KR 180 R2500 robot arm. The pultrusion pulling speed was 0.3 m/min, which is within the range of speeds of traditional pultrusion [25]. The UV source used was a Phoseon FireFlex UV LED, with an emitting window of 75 × 50 mm^2. The selected intensity was 8 W/cm^2 and the emission peak of this UV source is found at 395 nm (the composite was irradiated from both sides).

2.4. Mechanical characterisation

2.4.1. Quasi-static compression tests

Quasi-static compression tests were carried out at 10 mm/min of compression speed along 50 mm of collapse distance. The equipment used is an universal test machine (Instron 4206), equipped with 100 kN load cell. 3 specimens of each configuration were tested in order to ensure the repeatability of the tests. From the force-displacement curve, the following crashworthiness characteristics are calculated: the peak load, P_{max} (kN), which was obtained from the maximum force of the first peak; the mean load, P_{mean} (kN), which was determined by equation 1.

$$P_{mean} = \frac{\int_0^{l_{max}} P(l)\mathrm{dl}}{l_{max}} \quad (1)$$

where, l_{max} (m) is the total collapsed length.

The absorbed energy, A_e (kJ), which is the area under the load-displacement curve (equation 2).

$$A_e = \int_0^{l_{max}} P(l)\mathrm{dl} \tag{2}$$

The Specific Energy Absorption, *SEA* (kJ/kg), which is the absorbed energy per unit of crushed specimen mass, m_t, (kg) (equation 3).

$$SEA = \frac{\int_0^{l_{max}} P(l)\mathrm{dl}}{m_t} \tag{3}$$

The crush efficiency, η_c , which is the percentage ratio of the mean load to peak load (equation 4).

$$\eta_c = \frac{P_{mean}}{P_{max}} \cdot 100 \tag{4}$$

2.4.3. Dynamic compression tests

As the strain rate is not considered in quasi-static compression test, the satisfactory performance of the crash-boxes cannot be ensured [14]. Thus, the most appropriate test to validate these components is the dynamic compression test [14,26]. Two different dynamic compression tests were performed depending on the amount of energy to be dissipated by the specimen type (building block or crash-box):

- The dynamic compression tests for building blocks were performed using a Fractovis plus drop-weight test machine. In order to maintain the same collapse length, an impact mass of 35 kg was used for 1.5 mm thick specimens, while for 2 mm thick specimens the mass was 45 kg. The drop height of 1 m was used (maximum permitted by the test machine) for both thicknesses. A triaxial accelerometer (PCB 356B21) was attached to the tip of the impactor to record the acceleration-time response. Hence, from acceleration-time response other impact parameters, such as displacement, velocity and load can be obtained based on Newton's second law and kinematics [16,23].
- For the case of crash-boxes, the dynamic compression test was performed (Fig. 2) at Pimot facilities (Poland). In this case, a 350 kg impact trolley has been used for testing the crash-boxes. The specimens were attached to this impact trolley and impacted against a rigid wall at 37 km/h. The energy that the crash-box has to absorb is determined by the kinetic energy of the trolley (Newtonian kinetic energy equation):

$$E_K = \frac{1}{2} \cdot m \cdot v^2 \tag{5}$$

where, E_K is the kinetic energy that the trolley presents in the impact (kJ), which is the energy that the crash-box has to absorb; m is the mass of the trolley (kg); and v is the velocity of the trolley in the impact (m/s). The force-displacement curves have been obtained integrating the information recorded by the accelerometers of the trolley and from the data recorded by a high-speed video camera at 10,000 frames per second.

Insert Fig. 2

2.5. Broken fibre percentage (BFP) in crushing stage

All post-crushed specimens were treated following the procedure described in ASTM D3171-09 in order to burn the matrix and analyse the post-crushed glass-fibres. All broken fibres are removed leaving only those fibres which are not broken in each fibre layer. These glass fibre layers are weighed in an OHAUS GALAXY 110 electronic balance and the percentage of broken fibres within the collapsed length is calculated following the equation 6.

$$BFP = 100 \cdot \left(1 - \frac{w - \rho_L (l_T - l_C)}{\rho_L \cdot l_C} \right) \quad (6)$$

where, *BFP* is broken fibre percentage (%); *w* is the weight of the fibres that are not broken after crushing stage (g); ρ_L is the linear density of the glass fibre layer (g/mm); l_T is the overall length of the specimen (mm); and l_C is the collapsed length (mm).

3. Results and discussion

3.1. Compression tests – Building block

3.1.1. Quasi-static compression test – Building block

The building blocks were tested at low compression speeds in order to characterise the energy absorption capability and the effect of the thickness of the material. Fig. 3a shows a representative load-displacement curve obtained for both analysed thicknesses, where it can be noticed that after the initial peak force, the load converges to a lower mean value. Analysing the quasi-static compression tests, it can be noticed that all the specimens had a stable and progressive crushing collapse. In addition, two images (upper and bottom view) of each specimen type are presented in Fig. 3b and 3c, where the different deformation and fracture mechanisms can be observed:

- Axial splitting between fronts, which is geometry dependent.
- Axial crack propagation, where energy is absorbed spreading the axial crack progressively.
- Fibre breakage.

It must be pointed out that these mechanisms are found in all tested specimens.

Insert Fig. 3

Analysing the *SEA* and the efficiency values of both thicknesses (Table 1), it can be stated that the energy absorption capability of the specimens is similar within the experimental scatter. Regarding the peak and mean loads, 2 mm thick specimens present higher peak and mean load values, which is related to the higher resistant area. However, the dispersion of the values obtained from the 1.5 mm thick specimens is significantly higher compared to values obtained from 2 mm thick specimens. This fact could be due to the local buckling phenomena noticed in some 1.5 mm thick building blocks. Mamalis *et al.* [6,27] observed that the presence of local buckling areas during the collapse is more common in thinner composites. The local buckling reduces the load carrying capability of the specimen, and consequently the absorbed energy. Thus, it can be concluded that walls thinner than 1.5 mm are not recommended for the studied building blocks.

3.1.2. Dynamic compression test – Building block

Fig. 4a shows the representative load-displacement curves obtained from the accelerometer data of each composite thickness. Furthermore, as well as in quasi-static compression tests, two images (upper and bottom view) of each specimen type are presented (Fig. 4b and 4c).

Insert Fig. 4

Referred to deformation mechanisms, the same mechanisms and progressive collapse than in the quasi-static compression tests are identified in dynamic testing (axial splitting between fronts, axial crack propagation and fibre breakage). However, more extended delaminated areas and less fibre breakage have been identified as it is reported in Fig. 5. The building blocks tested at quasi-static compression rate present a significantly higher *BFP* (approximately 75%) compared to the building blocks tested at dynamic rates (approximately 40%). The reduction of broken fibres affects directly to the energy absorption capability as it was demonstrated by Esnaola *et al.* [28,29]. This reduction, which has been observed for both analysed thicknesses, can be explained due to the different predominant collapse modes of each tests. In quasi-static tests Mode I is the predominant collapse mode, which is associated with a large amount of energy absorption capability. This mode is described as a progressive crushing with microfragmentation of the composite and characterised by a wedge-shaped laminate with multiple longitudinal and interlaminar cracks [6,27,30]. In dynamic tests, instead, the predominant failure mode is a mixture of Mode I and Mode II. Where Mode II is described as an unstable local buckling of the

composite wall and delamination between plies. It is associated with low energy absorption capability [6,27,30]. The effect of the different predominant failure mode can be noticed when the results of the dynamic and quasi-static compression tests are analysed (Table 1). Although the peak load is similar for both crushing speeds, a clear reduction on the mean load can be observed for both thicknesses, approximately 40% for 1.5 mm and 35% for 2 mm. Consequently, the *SEA* value of 1.5 mm is reduced from 61.9 kJ/kg to 34.1 kJ/kg; and in the case of 2 mm, the reduction goes from 65.7 kJ/kg to 43.6 kJ/kg. Thus, it can be concluded that the increase of crushing speeds reduces the energy absorption capabilities of the building blocks with the studied geometry.

Insert Fig. 5

Insert Table 1

3.2. Compression tests – Crash-box

3.2.1. Crash-box design

The design factors to determine the absorbed energy by the cellular crash-box are the building block (material, geometry and thickness), the number and the length of building blocks and the number of crash-boxes in the vehicle. Hence, based on the results obtained from the quasi-static and dynamic compression tests of the building blocks and the kinetic energy of the trolley, an estimation of the length of a crash-box can be determined by the next equation:

$$l_{CB} = \frac{E_K}{n_{CB} \cdot n_B \cdot SEA_B \cdot \rho_{LB} \cdot 10^{-3}} \tag{7}$$

where, l_{CB} is the crash-box length (mm); n_{CB} is the number of crash-boxes; n_B is the number of building blocks; SEA_B is the *SEA* value obtained from the quasi-static or dynamic compression tests of the building blocks (kJ/kg); and ρ_{LB} is the linear density of the building block (kg/m).

Following the equation 7 the estimation of the minimum crash-box length (made of 10 building blocks) is presented in Fig. 6. As it can be observed, for the 1.5 mm thick crash-box, the minimum length can vary from 150 mm to 250 mm depending on the compression speed of the characterisation test. The same trend is observed for 2 mm of thickness, where the minimum length can vary from 100 mm to 150 mm. In order to ensure that the length of the crash-boxes will be enough for the dynamic tests, the maximum estimated length should be considered. Therefore, the length of the crash-box of 1.5 mm would be 250 mm; and 150 mm for the case of 2 mm. Additionally, the length of all crash-boxes was increased 50 mm in order to have enough free length to attach the components to the impact trolley.

Insert Fig. 6

3.2.2. Quasi-static compression test – Crash-box

Regarding the quasi-static compression tests performed to crash-boxes, Fig. 7a presents a representative load-displacement curve obtained for both analysed thicknesses. In this case, as the building block, all the crash-boxes had a stable and progressive crushing collapse. No differences are found in the load-displacement curve appearance (except higher values due to the combination of building blocks). Two images (upper and bottom view) of each specimen type are shown in order to analyse the deformation and fracture mechanisms (Fig.7b and 7c). Compared to the building block, the crash-box presents higher fibre breakage at quasi-static compression rate. This effect cannot be quantitatively analysed due to the size of the component and the available furnace. However, comparing the status of the specimens after testing, the higher level of *BFP* of the crash-box is evident (all the specimens were completely broken-down). This fact may be due to that Mode I collapse type is affected by the geometry of the crash-box, since the propagation of the axial crack and the splitting between fronts are hindered by the interaction with the adjacent building blocks. In this way, a slight decrease in *SEA* value (around 5%) is found for the crash-box (Table 2). Referred to the efficiency, a slight decrease is also noticed in the crash-box. That effect is due to the increase of the peak load, which is slightly higher than the sum of the individual peak load of each building block due to the higher stability of the crash-box. Additionally, the local buckling issues found in 1.5 mm thick building blocks are not identified in the crash-boxes.

Insert Fig. 7

3.2.3. Dynamic compression test – Crash-box

Once the length of the crash-box is estimated based on the compression tests of building blocks, the dynamic compression tests can be conducted. Figs. 8a and 9a show three representative load-deformation curves obtained from the accelerometer data of each composite thickness. In addition to the images of the after-crashing status of the specimens (Fig. 8b and Fig. 9b), four images of each component during the crash-test are presented (Fig. 8c and Fig. 9c). All the specimens had a stable and progressive collapse. Regarding the deformation mechanisms, the same mechanisms and progressive collapse than in the quasi-static compression tests are identified in dynamic testing. However, as it occurs in the case of the building block at dynamic rates, broken fibre percentage gets significantly reduced compared to quasi-static compression rates. Therefore, the energy absorption capability of the component is negatively affected. This fact is supported by analysing the values obtained from the dynamic test shown in Table 2. *SEA*

values are decreased from approximately 60 kJ/kg to 40-45 kJ/kg within the experimental scatter (for both thicknesses). However, it has to be mentioned that the *SEA* value measured for both thicknesses at dynamic rates is similar to the values obtained from 2 mm thick building blocks at dynamic rates. Regarding the peak and mean loads, a decrease close to 30% has been measured for almost all the specimens, which is largely related to the high presence of delamination instead of fibre breakage. As in quasi-static compression test, the peak load is close to the sum of the individual peak load of each building block.

Insert Fig. 8

Insert Fig. 9

Insert Table 2

Finally, Fig. 10 shows a graphical comparison of *SEA* values obtained from quasi-static and dynamic tests for all the specimens. It can be stated, that the energy absorption capability is decreased at dynamic compression rates. On the other hand, analysing the Fig. 10, it can be assumed that the estimation of the crash-box length cannot be done by quasi-static compression test, even with the same configuration of the cash-box. The failure mode is different at higher compression rates and consequently, high differences in *SEA* values are obtained. However, it can be noticed that *SEA* values between both configurations in the dynamic test are similar. This relation can be also identified analysing the maximum collapsed lengths of the crash-boxes (approximately 225 mm for the 1.5 mm thick crash-box and 125 mm for the 2 mm thick crash-box), which are very close with the prediction obtained from dynamic compression tests of building blocks. Therefore, in order to design a crash-box as a cellular component, the characterisation of the building block at dynamic compression rates can be performed. This fact implies the reduction of the costs during the design and validation stages of the crash-box. The dynamic test of the building block can be performed by a standard drop-weight test machine equipped with an accelerometer. The test of the crash-box instead, has to be performed in a facility able to crash the trolley (equipped with accelerometers) against a barrier at the required velocity. Hence, the equipment for testing the crash-box is more complex and expensive than the test of the building block. In addition, comparing the cost of the prototypes, the reduction in cost is even higher due to the crash-box is composed of building blocks (higher consumption in raw materials and assembly time).

Insert Fig. 10

4. Conclusions

In the present paper, a feasibility analysis of designing automotive composite crash structures as a cellular component based on the characterisation of the building block has been performed. The effect of testing velocity and thickness on the energy absorption capability has been analysed. These are the main conclusions:

- The *SEA* values of the building block and the crash-boxes are similar. Furthermore, the effect of testing velocity is also the same, since *SEA* values obtained from the dynamic compression tests are lower than the values from the quasi-static compression tests. This reduction can be attributed to the decrease of the mean load observed in the dynamic tests, since the change of predominant failure mechanisms from fibre breakage in quasi-static to delamination under dynamic conditions.
- Wall thickness is a critical parameter, since even using the same thickness in building blocks and crash-boxes, for thin wall designs remarkable differences can be found. The origin of the deviations is related to the fact that buckling is more probable testing the building block than testing the crash-boxes of the same wall thickness.
- The *SEA* values of the building block and the crash-box are similar when the characterisation is carried out with the same thickness and testing velocity, since deformation and fracture mechanisms are the same in each case. In the same way, the peak load of the crash-box can be estimated by multiplying the value of the building block and the number of units in the crash-boxes.

Therefore, it can be postulated that designing a crash-box as a cellular component is only feasible based on the dynamic compression tests of the building blocks. This fact can imply an important reduction in costs during the design and validation stages of the crash-box, due to the simplicity and low cost of the dynamic compression test of the building block in comparison with the test of the crash-box.

Acknowledgements

I. Saenz-Dominguez thanks the Basque Government for the grant (PRE_2015_1_0375) and for providing financial support (PUL3D UE 2015-2 & ICUV ZL-2016/00349; IT833-16; OF 188/2017) for this study. The authors also thank the European Commission for providing financial support (WEEVIL Ultralight and Ultrasafe Efficient Electric Vehicle - Grant agreement no.: 653926) for this study. Finally, the authors

want to thank *Przemysłowy Instytut Motoryzacji* (PIMOT) for providing their facilities to perform the crash-tests.

References

[1] Adam H. Carbon fibre in automotive applications. Mater Des 1997;18:349–55.

[2] Hull D. A Unified Approach to Progressive Crushing of Fiber-Reinforced Composite Tubes. Compos Sci Technol 1991;40:377–421.

[3] Thornton PH. Energy Absorption in Composite Structures. J Compos Mater 1979;13:247–62.

[4] Farley GL. Energy Absorption of Composite Materials. J Compos Mater 1983;17:267–79.

[5] Carruthers JJ, Kettle AP, Robinson AM. Energy absorption capability and crashworthiness of composite material structures: A review. Appl Mech Rev 1998;51:635.

[6] Mamalis AG, Manolakos DE, Ioannidis MB, Papapostolou DP. On the response of thin-walled CFRP composite tubular components subjected to static and dynamic axial compressive loading: Experimental. Compos Struct 2005;69:407–20.

[7] Ochelski S, Gotowicki P. Experimental assessment of energy absorption capability of carbon-epoxy and glass-epoxy composites. Compos Struct 2009;87:215–24.

[8] Ramakrishna S. Microstrucural design of composite materials of crashworthy structural applications. Mater Des 1997;18:167–73.

[9] Kakogiannis D, Chung Kim Yuen S, Palanivelu S, Van Hemelrijck D, Van Paepegem W, Wastiels J, et al. Response of pultruded composite tubes subjected to dynamic and impulsive axial loading. Compos Part B Eng 2013;55:537–47.

[10] Hamada H, Ramakrishna S. Scaling effects in the energy absorption of carbon-fiber/PEEK composite tubes. Compos Sci Technol 1995;55:211–21.

[11] Lau STW, Said MR, Yaakob MY. On the effect of geometrical designs and failure modes in composite axial crushing: A literature review. Compos Struct 2012;94:803–12.

[12] Mamalis AG, Manolakos DE, Demosthenous GA, Ioannidis MB. Analysis of failure mechanisms observed in axial collapse of thin-walled circular fibreglass composite tubes. Thin-Walled Struct 1996;24:335–52.

[13] Farely GL. Effect of specimen geometry on the energy absorption of composite materials. J Compos Mater 1986;20:390.

[14] Jacob GC, Fellers JF, Simunovic S, Starbuck JM. Energy absorption in polymer composites for automotive crashworthiness. vol. 36. 2002.

[15] Palanivelu S, Van Paepegem W, Degrieck J, Van Ackeren J, Kakogiannis D, Van Hemelrijck D, et al. Experimental study on the axial crushing behaviour of pultruded composite tubes. Polym Test 2010;29:224–34.

[16] Esnaola A, Ulacia I, Elguezabal B, Del Pozo de Dios E, Alba JJ, Gallego I. Design, manufacturing and evaluation of glass/polyester composite crash structures for lightweight vehicles A. Int J Automot Technol 2016;17:1013–22.

[17] Cheung KC, Gershenfeld N. Reversibly Assembled Cellular Composite Materials. Science (80-) 2013;341:1219–21.

[18] Tena I, Esnaola A, Sarrionandia M, Ulacia I, Torre J, Aurrekoetxea J. Out of die ultraviolet cured pultrusion for automotive crash structures. Compos Part B Eng 2015;79:209–16.

[19] Tena I, Sarrionandia M, Torre J, Aurrekoetxea J. The effect of process parameters on ultraviolet cured out of die bent pultrusion process. Compos Part B Eng 2016;89:9–17.

[20] Esnaola A, Tena I, Saenz-Dominguez I, Aurrekoetxea J, Gallego I, Ulacia I. Effect of the manufacturing process on the energy absorption capability of GFRP crush structures. Compos Struct 2018;187:316–24.

[21] Othman A, Abdullah S, Ariffin AK, Mohamed NAN. Investigating the quasi-static axial crushing behavior of polymeric foam-filled composite pultrusion square tubes. Mater Des 2014;63:446–59.

[22] Ramakrishna S. Energy absorption behaviors of knitted fabric reinforced composite tubes. J Reinf Plast Compos 1995;14:1121–41.

[23] Liu Q, Ou Z, Mo Z, Li Q, Qu D. Experimental investigation into dynamic axial impact responses of double hat shaped CFRP tubes. Compos Part B Eng 2015;79:494–504.

[24] Farley GL. Energy absorption of composite material and structure 1987.

[25] Suratno BR, Ye L, Mai YW. Simulation of temperature and curing profiles in pultruded composite rods. Compos Sci Technol 1998;58:191–7.

[26] Baguley P, Roy R, Watson J. Cost of physical vehicle crash testing. Proc 15th ISPE Int Conf Concurr Eng CE 2008 2008:18–22.

[27] Mamalis AG, Manolakos DE, Demosthenous GA, Ioannidis MB. The static and dynamic axial collapse of fibreglass composite automotive frame rails. Compos Struct 1996;34:77–90.

[28] Esnaola A, Ulacia I, Aretxabaleta L, Aurrekoetxea J, Gallego I. Quasi-static crush energy absorption capability of E-glass/polyester and hybrid E-glass-basalt/polyester composite structures. Mater Des 2015;76:18–25..

[29] Esnaola A, Tena I, Aurrekoetxea J, Gallego I, Ulacia I. Effect of fibre volume fraction on energy absorption capabilities of E-glass/polyester automotive crash structures. Compos Part B Eng 2016;85:1–7.

[30] Hadavinia H, Ghasemnejad H. Effects of Mode-I and Mode-II interlaminar fracture toughness on the energy absorption of CFRP twill/weave composite box sections. Compos Struct 2009;89:303–14.

Table 1. Results of building block compression tests.

Table 2. Results of crash-box compression tests.

Fig. 1. (a) Cross-section of the building block; (b) cross-section of the crash-box; (c) detail of out of die UV cured pultrusion machine.

Figure 2. Dynamic compression test of crash-box specimens at PIMOT facilities.

Fig. 3. (a) Load-displacement curve of quasi-static compression tests of building blocks; (b) 2 mm thick building block after quasi-static compression test (upper and bottom views); (c) 1.5 mm thick building block after quasi-static compression test (upper and bottom views).

Fig. 4. (a) Load-displacement curves from dynamic compression test of building blocks; (b)1.5 mm thick building block after dynamic compression test (upper and bottom views); (c) 2 mm thick building block after dynamic compression test (upper and bottom views).

Fig. 5. Comparison of different BFP of the specimens tested in quasi-static and dynamic conditions.

Fig. 6. Estimation of the minimum crash-box length: (a) 1.5 mm thick crash-box; (b) 2 mm thick crash-box.

Fig. 7. (a) Load-displacement curves from dynamic compression test of crash-boxes; (b) 2 mm thick crash-box after quasi-static compression test (upper and bottom views); (c) 1.5 mm thick crash-box after quasi-static compression test (upper and bottom views).

Fig. 8. (a) Load-displacement curves from dynamic compression test of 1.5 mm thick crash-boxes; (b) 1.5 mm thick crash-box after dynamic compression test (c) dynamic compression test sequence of 1.5 mm thick crash-box.

Fig. 9. (a) Load-displacement curves from dynamic compression test of 2 mm thick crash-boxes; (b) 2 mm thick crash-box after dynamic compression test; (c) dynamic compression test sequence of 2 mm thick crash-box.

Fig. 10. Results from quasi-static and dynamic compression tests of all the specimens.

Configuration	Specimen thickness (mm)	Compression rate	Energy absorption capability				
			SEA **(kJ/kg)**	P_{max} **(kN)**	P_{mean} **(kN)**	η_c **(%)**	**Failure Mode**
Building block	1.5	10 mm/min	61.9 ± 4.4	14.8 ± 2.0	11.8 ± 0.8	76 ± 6	I
Building block	2	10 mm/min	65.7 ± 0.9	21.9 ± 0.2	18.6 ± 0.2	85 ± 1	I
Building block	1.5	15 km/h	34.1 ± 1.0	13.4 ± 0.3	7.2 ± 0.4	54 ± 2	I, II
Building block	2	15 km/h	43. 6 ± 1.9	24.2 ± 1.5	12.2 ± 1.6	51 ± 5	I, II

Configuration	Specimen thickness (mm)	Compression rate	Energy absorption capability				
			SEA **(kJ/kg)**	P_{max} **(kN)**	P_{mean} **(kN)**	η_c **(%)**	**Failure Mode**
Crash-box	1.5	10 mm/min	56.6 ± 1.0	175.0 ± 5.0	123.7 ± 12.7	71 ± 5	I
Crash-box	2	10 mm/min	62.7 ± 2.2	258.4 ± 8.0	195.7 ± 3.0	75 ± 2	I
Crash-box	1.5	37 km/h	40.1 ± 2.6	123.3 ± 4.2	86.3 ± 9.3	69 ± 8	I, II
Crash-box	2	37 km/h	47.2 ± 4.1	229.5 ± 9.7	131.5 ± 5.3	57 ± 3	I, II

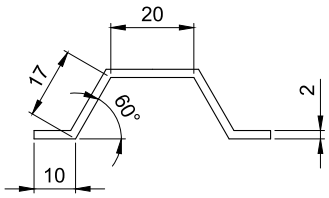

(a)

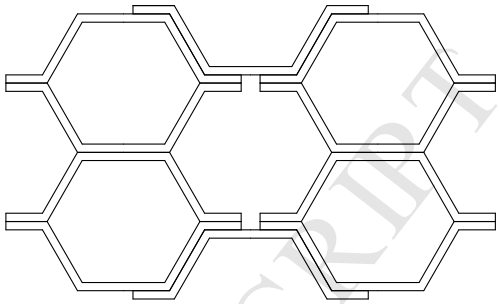

(b)

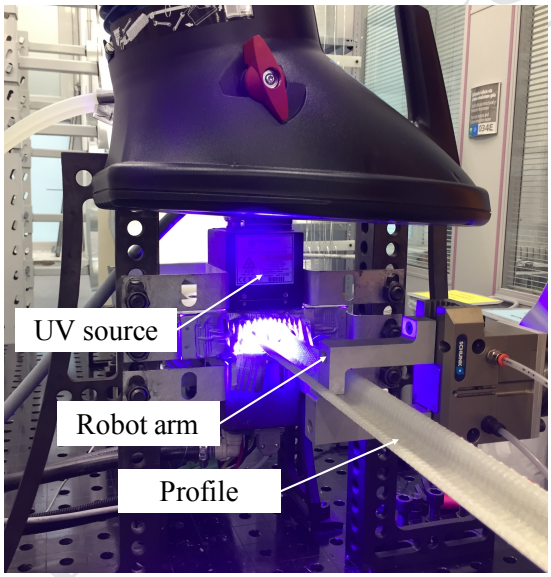

(c)

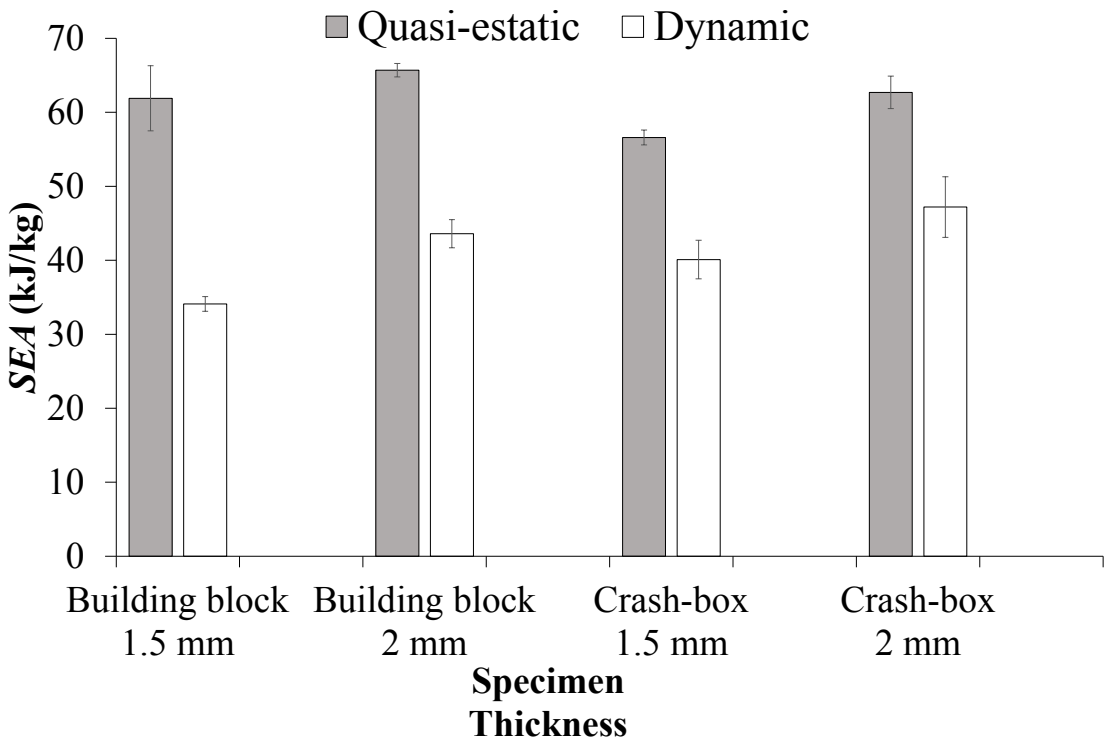

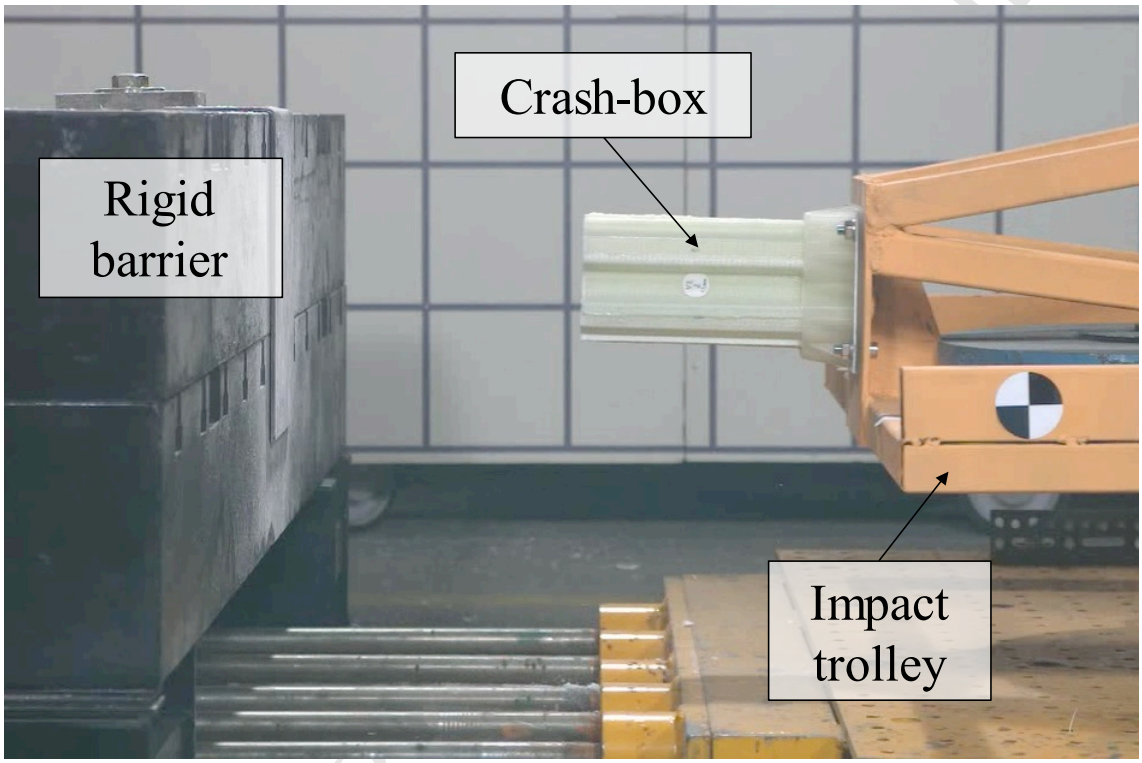

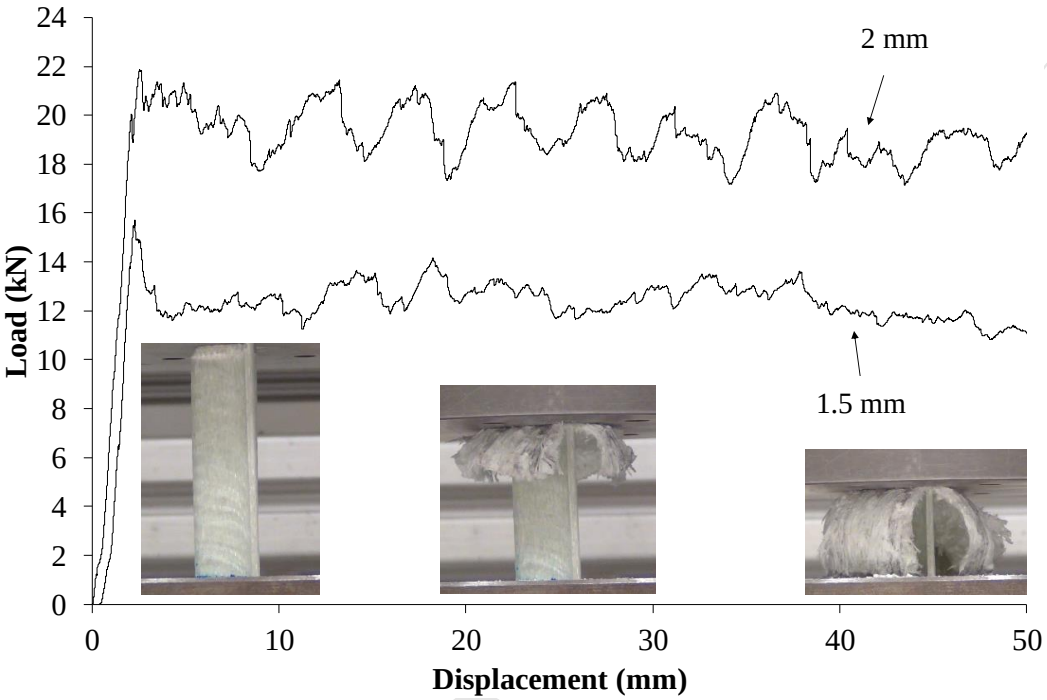

(a)

(b) (c)

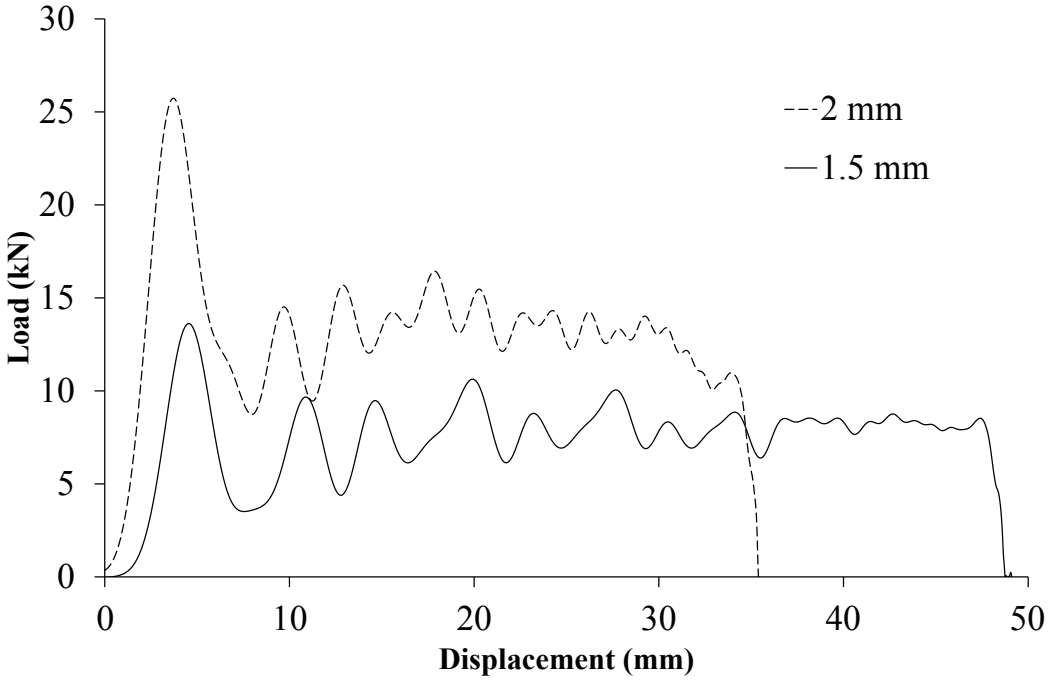

(a)

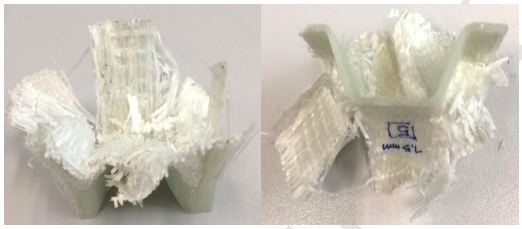

(b)

(c)

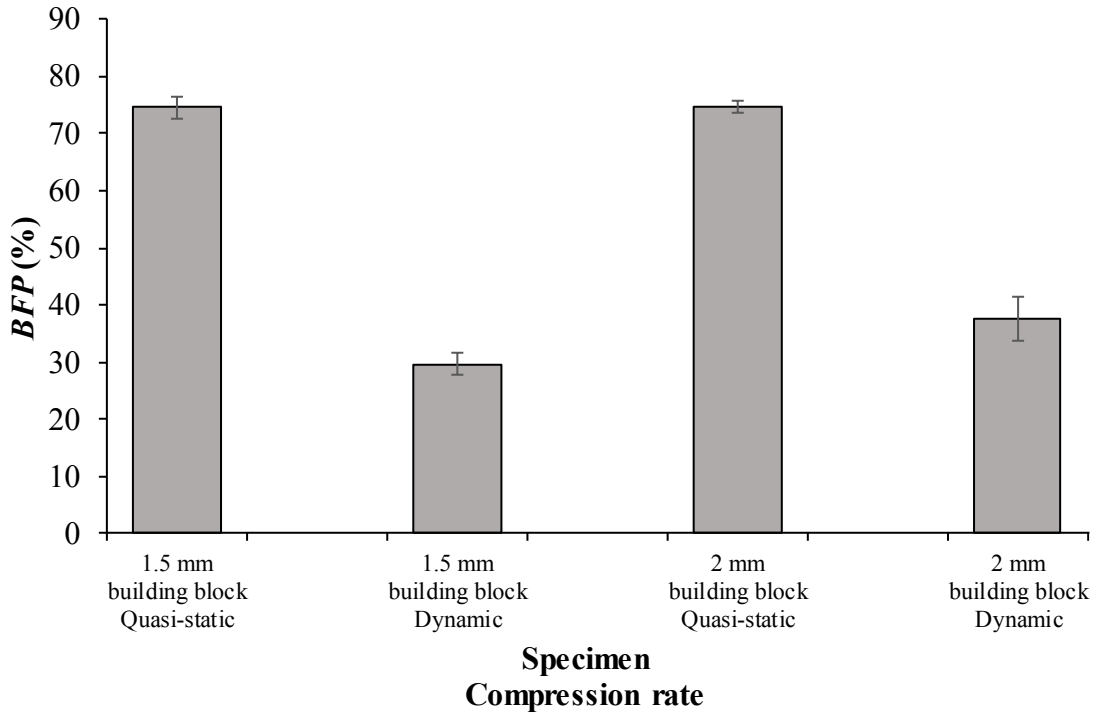

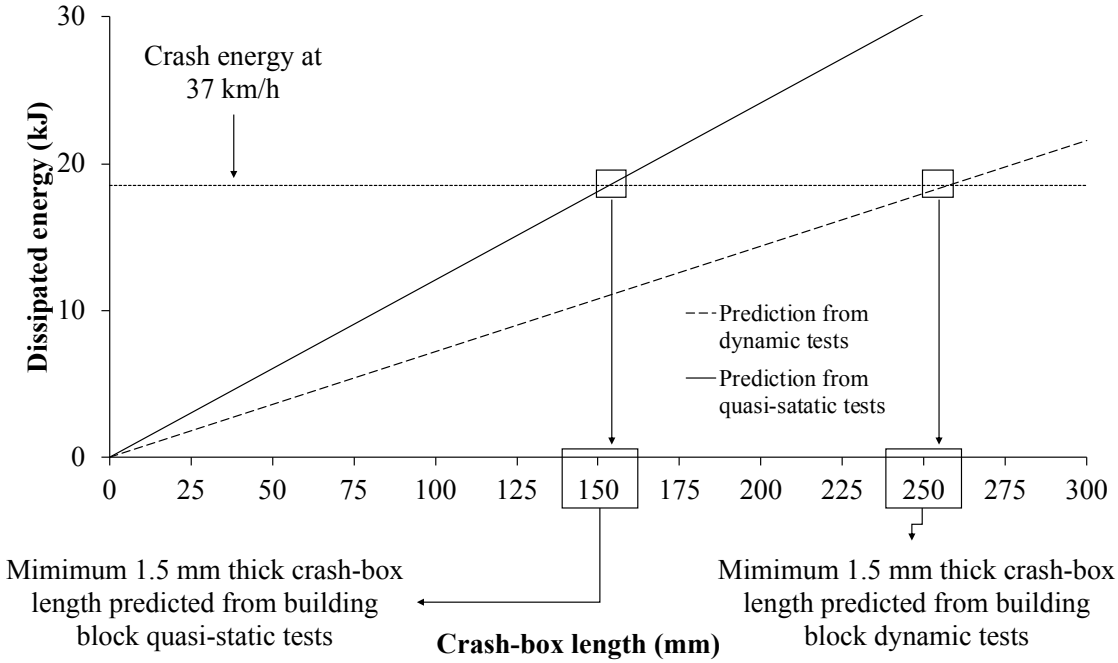
30
20
10
0
Dissipated energy (kJ)
Crash energy at
37 km/h
Prediction from
dynamic tests
Prediction from
quasi-satatic tests
0
25
50
75
100
125
150
175
200
225
250
275
300
Mimimum 1.5 mm thick crash-box
length predicted from building
block quasi-static tests
Mimimum 1.5 mm thick crash-box
length predicted from building
block dynamic tests
Crash-box length (mm)

(a)

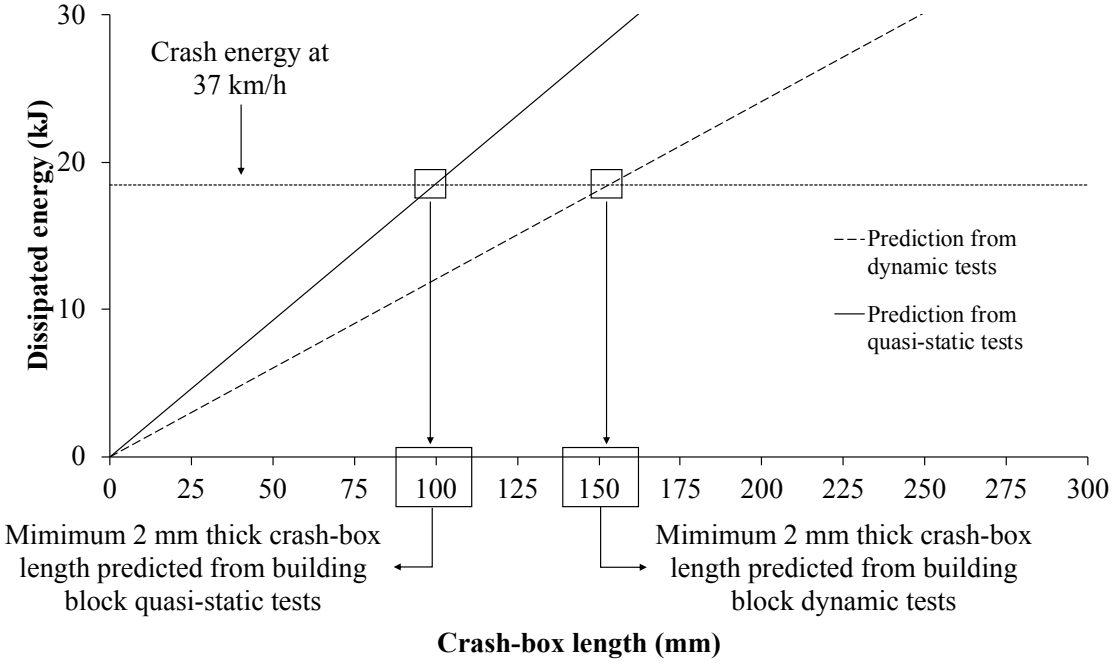
30
20
10
0
Dissipated energy (kJ)
Crash energy at
37 km/h
Prediction from
dynamic tests
Prediction from
quasi-static tests
0
25
50
75
100
125
150
175
200
225
250
275
300
Mimimum 2 mm thick crash-box
length predicted from building
block quasi-static tests
Mimimum 2 mm thick crash-box
length predicted from building
block dynamic tests
Crash-box length (mm)

(b)

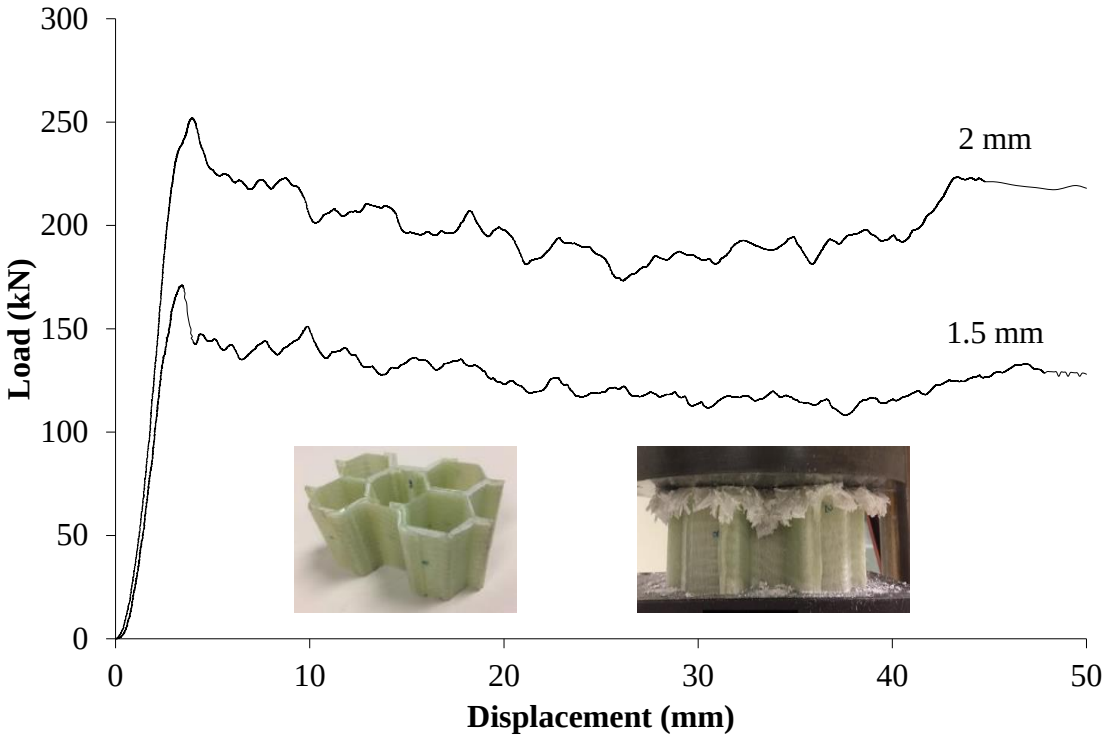

(a)

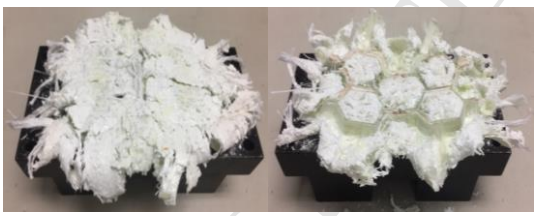

(b)

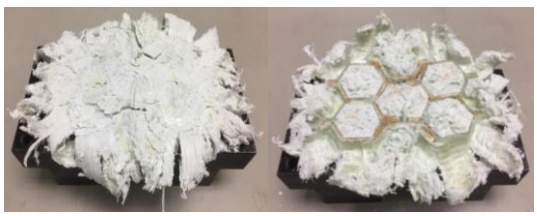

(c)

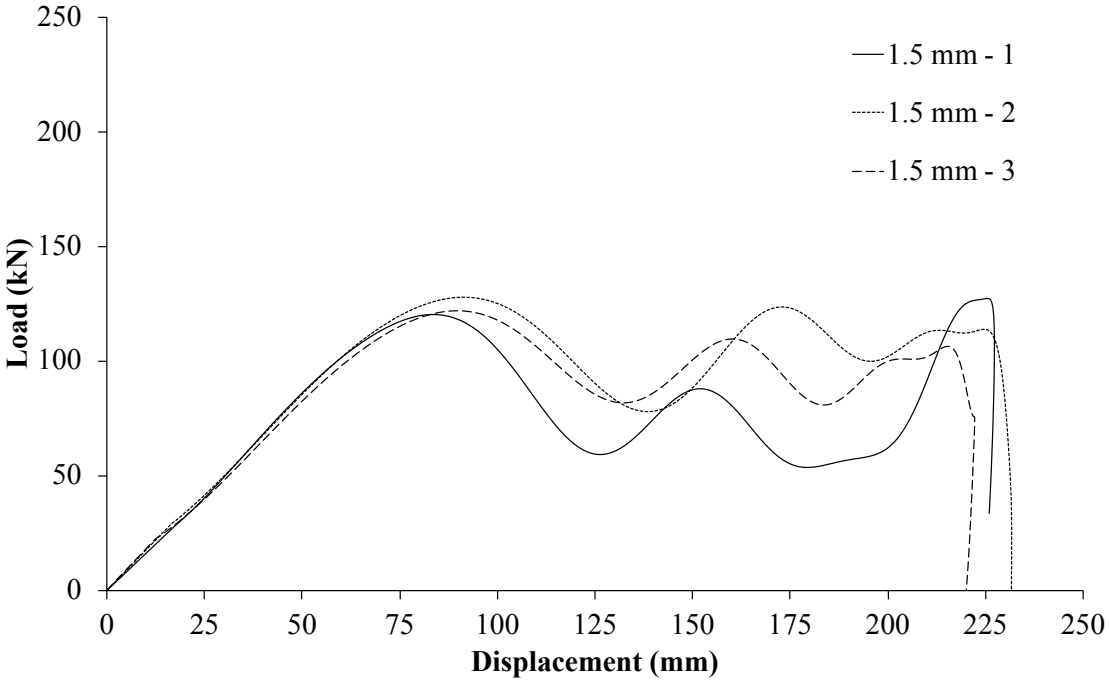
250
200
150
100
50
0
Load (kN)
0
25
50
75
100
125
150
175
200
225
250
Displacement (mm)
1.5 mm - 1
1.5 mm - 2
1.5 mm - 3

(a)

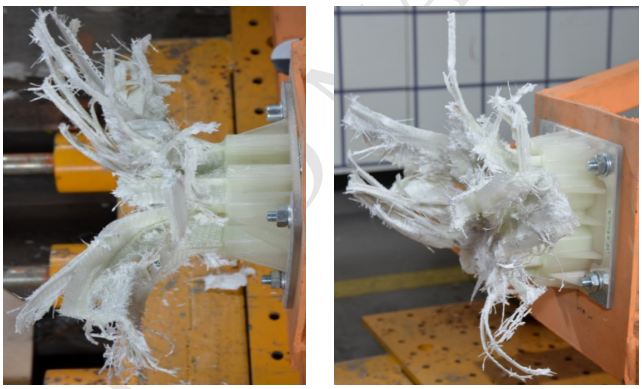

(b)

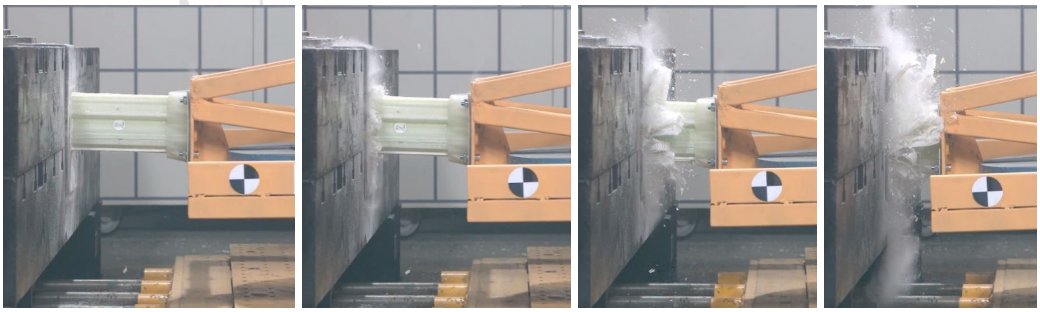

(c)

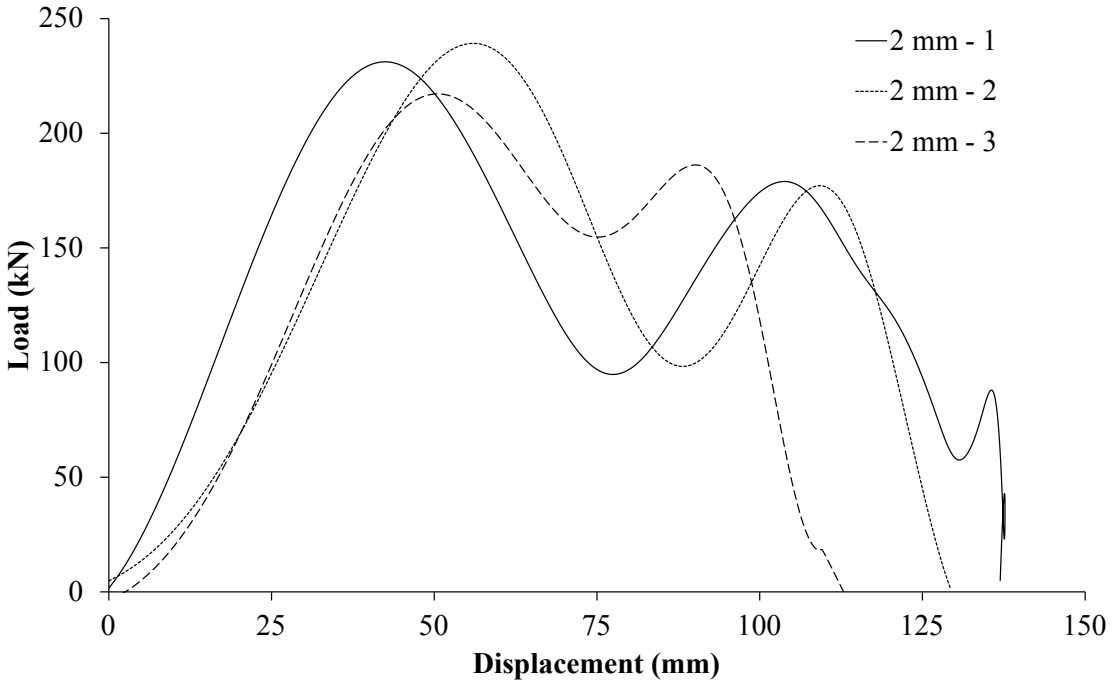
250
200
150
100
50
0
Load (kN)
0
25
50
75
100
125
150
Displacement (mm)
2 mm - 1
2 mm - 2
2 mm - 3

(a)

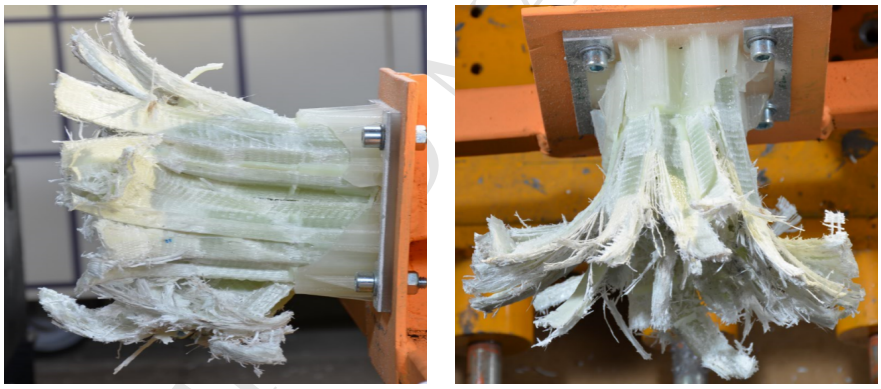

(b)

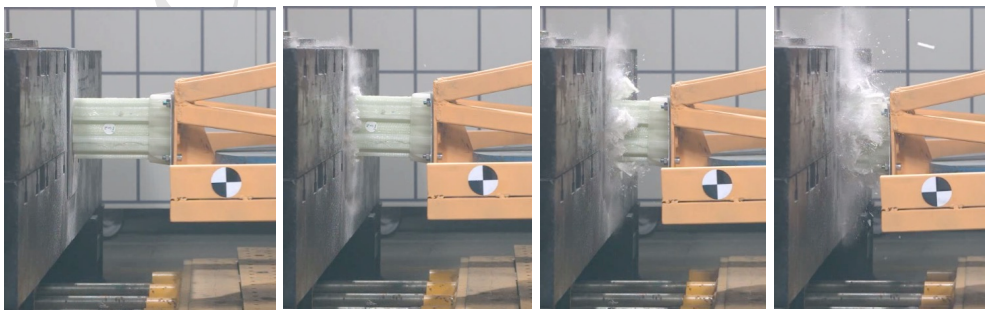

(c)